Journal of Hepatocellular Carcinoma

Dovepress
Taylor & Francis Group

Open Access Full Text Article

ORIGINAL RESEARCH

An Interpretable Radiomics-Based Model Using Susceptibility-Weighted Imaging for Non-Invasive Prediction of Tertiary Lymphoid Structures in Hepatocellular Carcinoma

Lizhen Liu[1,*], Fen Gao[1,*], Yiman Li[1,*], Jie Cheng[1,*], Huarong Zhang[2], Ping Cai[1], Wei Chen[1], Xiaoming Li[1]

[1]7T Magnetic Resonance Translational Medicine Research Center, Department of Radiology, Southwest Hospital, Army Medical University (Third Military Medical University), Chongqing, People's Republic of China; [2]Institute of Pathology and Southwest Cancer Center, Southwest Hospital, Third Military Medical University (Army Medical University), Chongqing, People's Republic of China

*These authors contributed equally to this work

Correspondence: Wei Chen; Xiaoming Li, Email landcw@tmmu.edu.cn; lxm359261069@tmmu.edu.cn

Background: Intratumoral tertiary lymphoid structures (iTLSs) are associated with favorable prognosis and immunotherapy response in hepatocellular carcinoma (HCC). This study aimed to develop an interpretable susceptibility-weighted imaging (SWI)-based radiomics model to non-invasively predict iTLSs in HCC.

Materials and Methods: A retrospective cohort of 477 HCC patients undergoing preoperative SWI was used (training: 290; validation: 125; independent validation: 62). Radiomics models were constructed using five machine learning algorithms: logistic regression, random forest (RF), support vector machine, extreme gradient boosting, and K-nearest neighbors. Model performance was evaluated using the area under the ROC curve (AUC), model interpretability was examined using shapley additive explanations (SHAP), and survival analyses were performed to assess clinical relevance.

Results: In the independent validation cohort, the RF algorithm was identified as the optimal classifier, with an AUC of 0.771 (95% CI: 0.641–0.883), sensitivity of 78.6%, and specificity of 67.6%. It significantly outperformed the radiological model ($p = 0.046$), and showed comparable performance with the hybrid model in predicting iTLSs positivity (iTLSs+) ($p > 0.05$). SHAP analysis showed that radiomics features (logarithm_firstorder_Minimum and exponential_glszm_ZoneEntropy) were significant predictors of iTLSs+. Kaplan-Meier analysis demonstrated improved time-to-recurrence (TTR) in the iTLSs+ predictor group compared to the iTLSs-negativity (iTLSs-) predictor group ($p < 0.05$). Furthermore, patients in the iTLSs+ predictor group receiving tyrosine kinase inhibitors combined with immune checkpoint inhibitors (TKI-ICI) therapy exhibited significantly extended TTR ($p < 0.05$), while no benefit was observed in the iTLSs- predictor group.

Conclusion: The SWI-based radiomics model provided a non-invasive tool for predicting iTLSs+ in HCC and identifying patients who might benefit from TKI-ICI therapy, and it showed potential for future integration into clinical decision-making workflows.

Keywords: hepatocellular carcinoma, susceptibility-weighted imaging, magnetic resonance imaging, radiomics, tertiary lymphoid structures

Background

Hepatocellular carcinoma (HCC) is the third leading cause of cancer-related death worldwide, with over 700,000 fatalities annually.[1] Despite surgical resection, nearly 70% of patients experience recurrence within five years, limiting long-term survival.[2] Recent advances in immune checkpoint inhibitor (ICI)-based therapies, such as atezolizumab plus bevacizumab, have improved clinical outcomes for HCC patients.[3] However, the high molecular and genetic heterogeneity of HCC poses challenges for optimal patient selection, leaving a critical gap in clinical practice.[4]

Received: 24 July 2025
Accepted: 23 September 2025
Published: 30 September 2025

Graphical Abstract

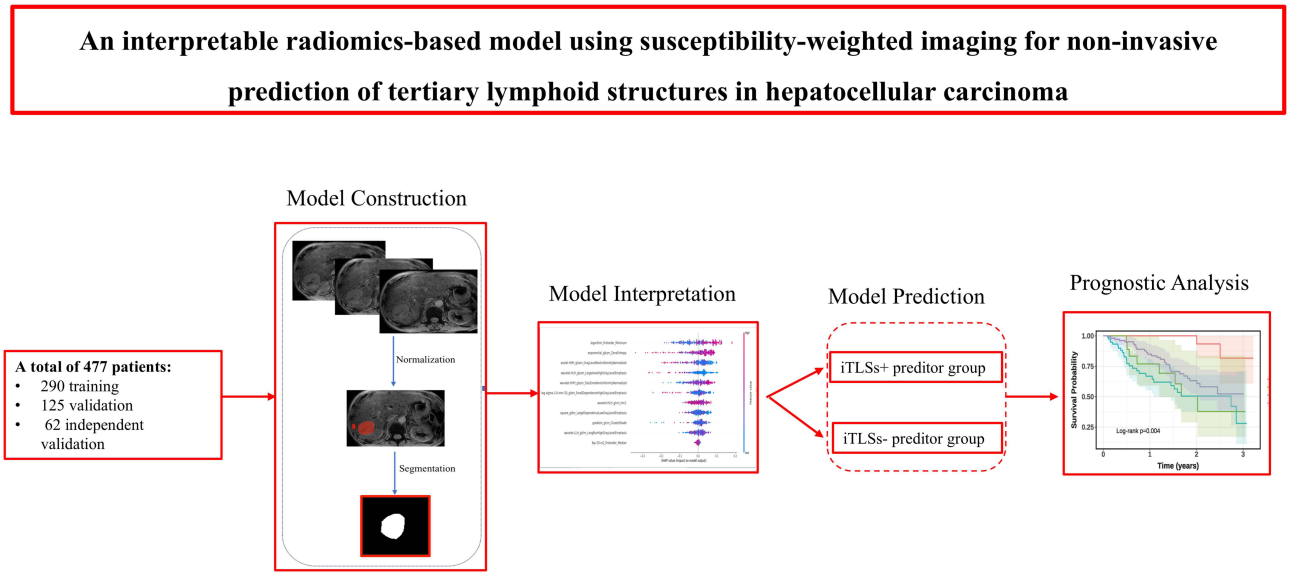

Recent studies have highlighted the tumor microenvironment (TME) as a critical factor in tumor behavior and response to treatment.[5,6] Tertiary lymphoid structures (TLSs), comprising lymphoid aggregates within the tumor, facilitate immune cell interactions, antigen presentation, and activation, potentially promoting anti-tumor immunity.[7] In HCC, the presence of intratumoral TLSs (iTLSs) may be a prognostic and predictive biomarker for patients with HCC receiving ICI, with their presence often associated with improved outcomes and enhanced immune response.[8] The prediction of iTLSs optimizes treatment planning after surgery, reduces recurrence risk, and enhances patient outcomes. However, their non-invasive identification of iTLSs remain challenging.

Several studies have identified intratumoral hemorrhage as a potential predictor of iTLSs in HCC,[9,10] possibly because hemorrhage leads to red blood cell lysis and the release of heme, iron metabolites, and other Damage-Associated Molecular Patterns (DAMPs), which may reshape the immune microenvironment and modulate TLS formation.[11,12] Previous studies in HCC have primarily relied on CT or conventional MRI sequences, such as diffusion-weighted or contrast-enhanced imaging, but these modalities are limited in accurately capturing hemorrhagic information. Susceptibility-weighted imaging (SWI), a sensitive modality for detecting endogenous susceptibility contrast agents like iron, hemoglobin, and hemosiderin, has shown high accuracy in identifying microhemorrhages in HCC,[13–15] underscoring its potential for iTLSs prediction. However, visual assessment of SWI remains limited by subjectivity and difficulty in detecting subtle hemorrhages. Radiomics can overcome these limitations by extracting high-dimensional quantitative features from imaging data, enabling objective biomarker identification.[16] To date, few studies have explored SWI-based radiomics for predicting iTLSs in HCC.

This study proposes an interpretable SWI-based radiomics model for predicting iTLSs-positivity (iTLSs+) in HCC. Shapley additive explanations (SHAP) were used to enhance model interpretability, and model-based stratification was applied to analyze time-to-recurrence (TTR), offering a novel tool for precision management.

Materials and Methods

Study Population

This study was conducted in accordance with the guidelines of the Declaration of Helsinki and was approved by the Institutional Review Board of the Army Medical University (Approval No.: KY2023107). As this was a retrospective

study, the requirement for informed consent was waived. The study was registered in the Research Registry (researchregistry10321).

Patients with histologically confirmed HCC who underwent surgical resection between June 2021 and October 2024 at Army Medical University were included. Inclusion criteria were: 1) preoperative SWI performed within 1 month prior to surgery; 2) complete clinical and pathological. Exclusion criteria included: 1) incomplete or poor-quality SWI images; 2) evidence of extrahepatic metastasis. 3) a past treatment history involving local regional or systemic anticancer therapies directed at the liver. Patients meeting the inclusion and exclusion criteria were randomly assigned into a training cohort (70%) and a validation cohort (30%). In addition, an independent validation cohort was included.

Clinical and laboratory information was collected, including demographic data (age and sex), etiology of liver disease, quantification of Hepatitis B virus DNA (HBV-DNA), history of antiviral treatment, liver function and coagulation profiles, as well as complete blood counts such as white blood cell (WBC) and platelet levels. Additional parameters recorded were alpha-fetoprotein (AFP) levels, tumor stage based on the Barcelona Clinic Liver Cancer (BCLC).

Based on factors related to a high risk of recurrence after surgery,[17] 77 patients with HCC in the training and validation cohorts received tyrosine kinase inhibitors (TKI) combined with ICI (TKI-ICI) therapy. The ICI used in this cohort included sintilimab and tislelizumab etc, both of which are programmed death-1 (PD-1) inhibitors commonly utilized for HCC. For TKI, lenvatinib and donafenib were the primary agents chosen. TKI-ICI were selected based on price, reimbursement, local health insurance and patient preference.

Patients underwent routine follow-up evaluations every 3–6 months post-surgery. Follow-up assessments included at least one imaging modality, such as contrast-enhanced CT, MRI, or ultrasound. The follow-up period extended until December 31, 2024. TTR was defined as the interval from the date of surgery to the detection of tumor recurrence. Recurrence was identified based on the presence of characteristic radiological findings, including non-rim arterial phase hyperenhancement and non-peripheral washout in the venous or delayed phase.[18]

MRI Protocols

MRI examinations were conducted using 3.0-T systems, incorporating sequences such as T2-weighted imaging, in-phase and opposed-phase imaging, and T1-weighted 3D volume-interpolated body examination (VIBE) with fat suppression. Gadoxetate disodium (Gd-EOB-DTPA) was administered at a dose of 0.025 mmol/kg with an injection rate of 1.0 mL/s, followed by a 30-mL saline flush. Upon detecting contrast arrival at the aortic arch, patients held their breath while the arterial phase (AP) scan was acquired. Subsequently, portal venous phase (PVP) and transition phase scans were performed at 55–70 seconds and 150–180 seconds post-injection, respectively. SWI acquisition was conducted with a flip angle of 20°, TR/TE of 150/10 ms, and a breath-hold of 16–21 s repeated thrice. The scan parameters included a FOV of 380×285 mm, matrix size of 384 × 187, 30 slices, and a slice thickness of 5.5 mm. The hepatobiliary phase (HBP) scan was conducted 15 minutes after contrast administration.

Subjective Assessment

Imaging features were visually assessed by three radiologists (Y.M.L., F.X.C, and P.C., with 11, 11, and 30 years of experience in abdominal imaging), blinded to all patient's clinical, pathology and outcomes, imaging features and definitions could be found in the Supplementary Table S1. If there was any disagreement, the opinion of the senior radiologist (P.C.) was adopted.

Histopathological Analysis

All histopathology slides (20×magnification) were digitally scanned and independently evaluated by two experienced liver pathologists (H.Z., and Q.L., with 22 and 10 years of experience in liver histopathology), blinded to clinical and imaging data. Discrepancies were resolved by consensus. For each case, iTLSs assessment was performed on at least five H&E-stained slides (range: 5–12). iTLSs were categorized into three stages:[19] (1) lymphoid aggregates—dense clusters of >100 lymphoid cells without clear boundaries at low magnification; (2) primary follicles—rounded lymphocyte

clusters lacking germinal centers; and (3) secondary follicles—mature iTLSs with fully developed germinal centers. Cases with any iTLSs were defined as iTLSs+, and those without as iTLSs-.

Image Segmentation and Radiomics Feature Extraction

The Pyradiomics Python package was used to extract radiomic features from the SWI sequence. The features extracted include: shape-based (16 features), first-order statistics (19 features), and texture features (75 features). The texture features were further divided into 24 features from the Gray Level Co-occurrence Matrix (GLCM), 16 from the Gray Level Run Length Matrix (GLRLM), 16 from the Gray Level Size Zone Matrix (GLSZM), 5 from the Neighboring Gray Tone Difference Matrix (NGTDM), and 14 from the Gray Level Dependence Matrix (GLDM). A total of 1616 radiomics features were extracted from each SWI sequence.

We devised a three-step program for dimensional reduction and robust feature selection. First, the volume of interest (VOI) segmentation was performed on the SWI sequence by two experienced abdominal radiologists (J.C. and X.M.L., with 11 and 12 years of experience, respectively) who were blinded to the clinical and pathologic details, using ITK-SNAP software. To assess inter-observer variability, 60 randomly selected cases were independently re-segmented by both radiologists, and intraclass correlation coefficients (ICCs) were calculated. Intra-observer reproducibility was further evaluated by repeating the segmentation of the same cases after a 4-week interval. Only features with both inter- and intra-observer ICCs > 0.75 (excellent stability) were retained for subsequent analysis. Second, all feature lines were standardized by the *z* score standardization method, and the correlation between features was calculated by the Spearman correlation coefficient. Third, the least absolute shrinkage and selection operator logistic regression algorithm (LASSO) was then applied, with penalty parameter tuning performed using 10-fold cross-validation. Features with non-zero coefficients were selected from the training cohort. The radiomics score (Radscore) used a linear combination of features selected for each patient, weighted according to their respective coefficients.

The Radscore was calculated for each patient by using the following equation:

$$Radscore = \sum_{i=1}^{n} c_i x_i + b$$

Where b was the intercept, x_i was the value of the ith selected feature, and c_i was the coefficient of the ith selected feature.

Model Development and Validation

Five machine learning (ML) algorithms—logistic regression (LR), random forest (RF), support vector machine (SVM), extreme gradient boosting (XGBoost), and K-nearest neighbors (KNN)—were used to construct predictive models based on the training set. Detailed model parameters are provided in the Supplementary Methods. Model discrimination was evaluated using receiver operating characteristic (ROC) curves and the area under the curve (AUC), along with sensitivity, specificity, accuracy, positive predictive value (PPV), negative predictive value (NPV), and F1-score. The ML algorithm with the highest AUC in the independent validation cohort was selected as the final radiomics model. The study workflow is illustrated in Figure 1.

In the training cohort, multivariate regression identified radiological variables associated with iTLSs+, forming the radiological model. A hybrid model combining radiomics and radiological models was then developed. The predictive performances of the radiomics, radiological, and hybrid models were compared across the training, validation, and independent validation cohorts.

Model Interpretation

Model interpretation was performed using SHAP, implemented through the Python SHAP package (version 2.0.0). SHAP, as a game theory-based model interpretation method, quantifies the contribution of each radiomic feature to the prediction of iTLSs.[20] By calculating and visualizing the influence of each feature on the model's predictions, SHAP provides transparent, intuitive, and clinically meaningful insights into the decision-making process of the model.

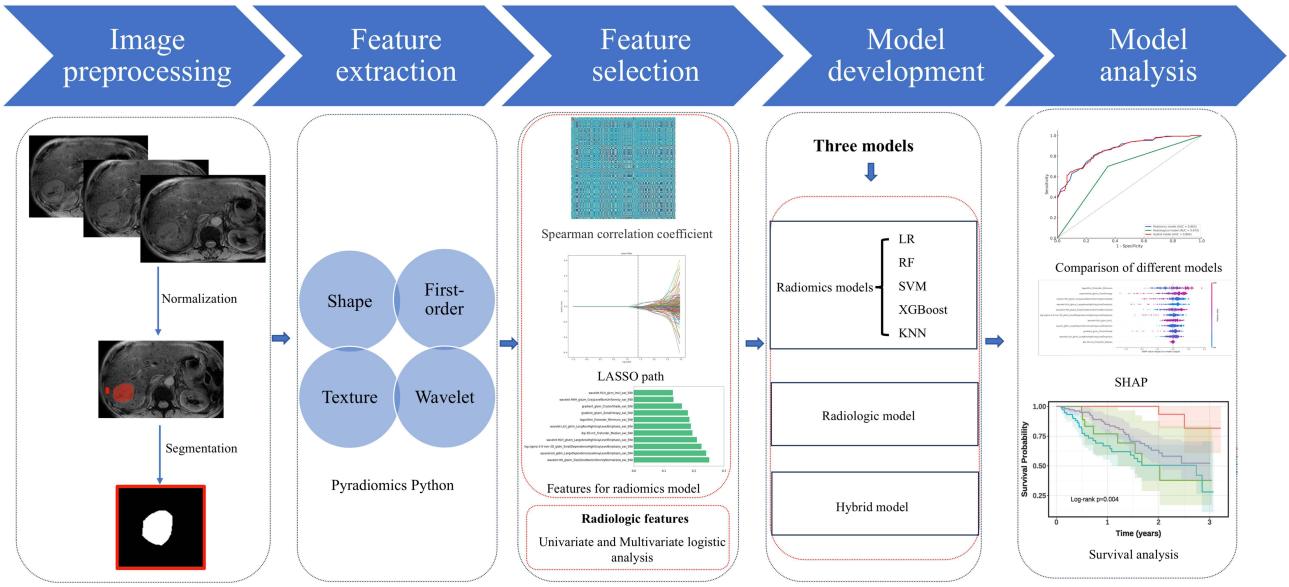

Figure 1 Overview of the workflow in our study.
Abbreviations: LASSO, least absolute shrinkage and selection operator; LR, logistic regression; RF, random forest; SVM, support vector machine; XGBoost, extreme gradient boosting; KNN, K-Nearest Neighbors; SHAP, shapley additive explanations.

Statistical Analysis

Data were analyzed using SPSS (version 21.0) and MedCalc (version 20.022). Inter-reader reliability was assessed using Fleiss' kappa, with values interpreted as slight (0.00–0.20), fair (0.21–0.40), moderate (0.41–0.60), substantial (0.61–0.80), or almost perfect agreement (0.81–1.00).[21] Categorical variables were presented as percentages, and continuous variables as mean ± standard deviation ($\bar{X} \pm S$) or median (interquartile range), according to the Shapiro–Wilk test for normality. The Mann–Whitney *U*-test or chi-square test was applied for group comparisons, as appropriate. The model's predictive performance for iTLSs+ was evaluated using the AUC with 95% confidence intervals (CI), and differences between AUCs were compared using DeLong's test. Patients were classified into iTLSs+ and iTLSs− predictor groups according to the optimal cutoff defined by the Youden index. Kaplan-Meier survival analysis with Log rank tests was used to compare survival outcomes. In the training cohort, cox regression was used to evaluate the associations of the Radscore and clinical variables (eg, age, gender, BCLC stage et. al) with TTR. Univariate analyses were first performed, and variables with $p < 0.10$ together with the Radscore were entered into the multivariate model using the Enter method to calculate hazard ratios (HRs) and 95% CI. A two-tailed p-value < 0.05 was considered statistically significant. A post-hoc power analysis was further performed to evaluate whether the sample size was sufficient to detect the observed discrimination performance of the radiomics model. Statistical power for the AUC was estimated under the null hypothesis AUC = 0.5, using the observed AUC and sample size, with a two-sided $\alpha = 0.05$.

Results

Clinical Characteristics and MRI Features of Patients

A total of 477 HCC patients (406 males) were enrolled. Of these, 415 patients met all criteria and were randomly divided into the training cohort (n = 290) and validation cohort (n = 125), with an additional 62 patients included as the independent validation cohort (Figure 2).

Baseline clinical characteristics across the training, validation, and independent validation cohorts were comparable, with no significant differences observed (all $p > 0.05$; Table 1). Similarly, within the training cohort, characteristics remained balanced between iTLSs+ and iTLSs- groups (all $p > 0.05$; Table 2).

Inter-rater agreement for imaging features was substantial to perfect (Fleiss' $\kappa = 0.636–0.846$; Supplementary Table S2). In univariate analysis, tumor size (p = 0.018), intratumor artery (p = 0.016), and intratumor hemorrhage ($p < 0.0001$) were

https://doi.org/10.2147/JHC.S551462

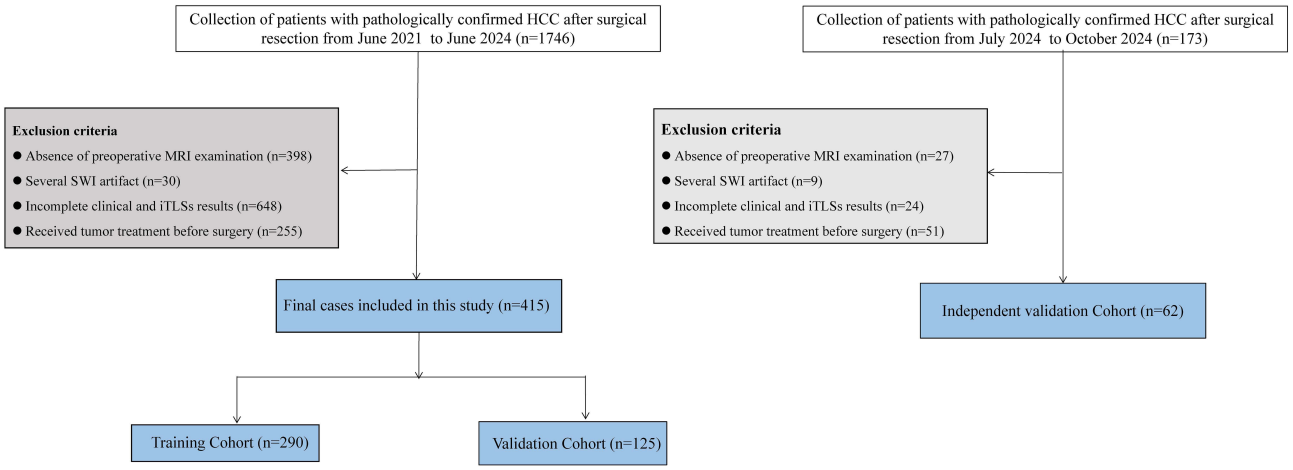

Figure 2 Flowchart of cohort selection.

associated with iTLSs+. However, multivariate analysis identified intratumor hemorrhage as the only independent predictor (OR = 0.231, 95% CI: 0.140–0.380, p < 0.001; Table 3), and it was used to build the radiological model.

Development and Validation of Radiomics Model

From the 1616 radiomic features initially extracted from the SWI sequence, 11 key features were ultimately selected as predictors of iTLSs+ (Supplementary Figure S1). Among the five ML algorithms, the RF algorithm consistently showed superior predictive ability in independent validation cohort, resulting in an AUC value of 0.771 (95% CI: 0.641–0.884) (Figure 3 and Table 4). Accordingly, a radiomics model was subsequently developed based on the RF algorithm.

In the overall cohort (n=477), a post hoc power analysis demonstrated that the study was adequately powered (power >99.9%) to detect the observed predictive performance (AUC = 0.828, P < 0.05).

Performance of Hybrid, Radiomics, and Radiological Models in Predicting iTLSs+ Across Cohorts

In the training cohort, the hybrid model and radiomics model for predicting iTLSs+ achieved AUC of 0.864 (95% CI: 0.823–0.903) and 0.863 (95% CI: 0.822–0.902), outperformed radiological model (AUC = 0.675, 95% CI: 0.617–0.730) (p < 0.0001, < 0.0001).

In the validation cohort, the hybrid model and radiomics model achieved AUC of 0.778 (95% CI: 0.689–0.859) and 0.764 (95% CI: 0.669–0.848), outperformed radiological model (AUC = 0.629, 95% CI: 0.540 to 0.713) (p = 0.008, = 0.023).

In the independent cohort, the hybrid model and radiomics model achieved AUC of 0.777 (95% CI: 0.654–0.883) and 0.771 (95% CI: 0.641–0.884), outperformed radiological model (AUC = 0.606, 95% CI: 0.488 to 0.728) (p = 0.046, = 0.013). In all cohorts, there were no significant differences between the hybrid model and the radiomics model (all p > 0.05) (Figure 4).

Model Interpretability

SHAP analysis provided quantitative insights into the radiomics model for predicting iTLSs+. The SHAP values for each feature were shown through variance importance, summary, and force plots to highlight their impact (Figure 5). We depicted the summary plot of SHAP value, which explained the impact of each feature on the model predictions. Among the features, the SHAP importance map showed the importance of each feature. The results showed logarithm_firstorder_Minimum and exponential_GLSZM_ZoneEntropy contributed the most to the RF algorithm.

Table 1 Baseline Characteristics of Patients in the Training, Validation, and Independent Validation Cohorts

Characteristic	Groups			p
	Training Cohort (n = 290)	Validation Cohort (n = 125)	Independent Validation Cohort (n = 62)	
Age	54 ± 11	57 ± 11	55 ± 11	0.219
Sex				0.255
Male	245 (84.5%)	104 (83.2%)	57 (91.9%)	
Female	45 (15.5%)	21 (16.8%)	5 (8.1%)	
History of antiviral				0.105
No	177 (61.0%)	70 (56.0%)	29 (46.8%)	
Yes	113 (39.0%)	55 (44.0%)	33 (53.2%)	
Etiology				0.533
HBV	249 (85.9%)	112 (89.6%)	52 (83.9%)	
Alcohol	16 (5.5%)	5 (4.0%)	2 (3.2%)	
HCV	5 (1.7%)	0 (0.0%)	2 (3.2%)	
Other	20 (6.9%)	8 (6.4%)	6 (9.7%)	
HBV-DNA replication≥10^3				0.492
No	188 (64.8%)	84 (67.2%)	45 (72.6%)	
Yes	102 (35.2%)	41 (32.8%)	17 (27.4%)	
TBIL (μmol/L)	15 (12, 20)	15 (12, 19)	14 (12, 18)	0.774
Albumin (g/L)	41.8 ± 3.9	41.1 ± 4.9	41.0 ± 3.6	0.249
AST (U/L)	32 (24, 41)	36 (26, 48)	31 (26, 51)	0.073
ALP (U/L)	92 (76, 114)	98 (74, 120)	88 (70, 114)	0.257
APTT (s)	27.57 ± 2.36	27.33 ± 2.51	28.18 ± 2.33	0.073
PT (s)	11.56 ± 0.79	11.72 ± 1.09	11.75 ± 0.78	0.124
FIB (s)	2.47 (2.07, 3.24)	2.36 (2.02, 2.91)	2.59 (2.15, 2.99)	0.254
TT (s)	18.74 ± 1.39	18.81 ± 1.22	18.87 ± 1.48	0.735
WBC (x10^{9}g/L)	5.29 (4.39, 6.13)	5.26 (4.30, 6.73)	6.03 (4.74, 6.84)	0.070
PLT (x10^{9}g/L)	162 ± 69	153 ± 64	166 ± 43	0.314
AFP>400ng/mL				0.158
No	212 (73.1%)	95 (76.0%)	39 (62.9%)	
Yes	78 (26.9%)	30 (24.0%)	23 (37.1%)	
BCLC stage				0.296
0	41 (14.1%)	22 (17.6%)	7 (11.3%)	
A	187 (64.5%)	73 (58.4%)	40 (64.5%)	
B	25 (8.6%)	10 (8.0%)	10 (16.1%)	
C	37 (12.8%)	20 (16.0%)	5 (8.1%)	

Abbreviations: HBV, hepatitis B virus; HCV, hepatitis C virus; HBV-DNA, hepatitis B virus-deoxyribonucleic acid; TBIL, total bilirubin; ALP, alkaline phosphatase; AST, aspartate aminotransferase; ALT, alanine aminotransferase; APTT, activated partial thromboplastin time; PT, prothrombin time; FIB, fibrinogen; TT, thrombin time; WBC, white blood cells; PLT, platelet; AFP, alpha-fetoprotein; BCLC, Barcelona Clinic Liver Cancer.

Association Between the Radiomics Model and Outcomes

The 1-, 2-, and 3-year survival rates were 80.1%, 62.3%, and 46.6% in the training cohort, and 83.7%, 62.9%, and 48.2% in the validation cohort. A total of 77 HCC patients received TKI-ICI therapy (51 in the training cohort and 26 in the validation cohort).

Univariate Cox regression analysis showed that both BCLC stage (HR = 1.502, 95% CI: 1.117–2.020, p = 0.007) and the Radscore (HR = 0.059, 95% CI: 0.011–0.301, p = 0.001) were significantly associated with TTR. Multivariate analysis demonstrated that the Radscore (HR = 0.120, 95% CI: 0.020–0.706, p = 0.019) and postoperative TKI-ICI therapy (HR = 2.158, 95% CI: 1.076–4.328, p = 0.030) remained independent predictors of TTR.

Using the cutoff from the radiomics model, patients were stratified into iTLSs+ and iTLSs- predictor groups. Kaplan-Meier analysis showed that in both cohorts, the iTLSs+ predictor group without TKI-ICI therapy had significantly longer

https://doi.org/10.2147/JHC.S551462

Table 2 Comparison of Baseline Characteristics Between iTLSs-Negativity and iTLSs-Positivity Croups in Different Cohorts

Characteristic	Training Cohort, n = 290			Validation Cohort, n = 125			Independent Validation Cohort, n = 62		
	iTLSs- n = 120	iTLSs+ n = 170	p	iTLSs- n = 45	iTLSs+ n = 80	p	iTLSs- n = 34	iTLSs+ n = 28	p
Age	56 ± 11	54 ± 11	0.087	56 ± 10	57 ± 11	0.522	54 ± 12	55 ± 10	0.617
Sex			0.650			0.202			>0.999
Male	100 (83.3%)	145 (85.3%)		40 (88.9%)	64 (80.0%)		31 (91.2%)	26 (92.9%)	
Female	20 (16.7%)	25 (14.7%)		5 (11.1%)	16 (20.0%)		3 (8.8%)	2 (7.1%)	
History of antiviral			0.300			0.409			0.284
No	69 (57.5%)	108 (63.5%)		23 (51.1%)	47 (58.8%)		18 (52.9%)	11 (39.3%)	
Yes	51 (42.5%)	62 (36.5%)		22 (48.9%)	33 (41.3%)		16 (47.1%)	17 (60.7%)	
Etiology			0.061			0.139			0.024
HBV	97 (80.8%)	152 (89.4%)		37 (82.2%)	75 (93.8%)		25 (73.5%)	27 (96.4%)	
HCV	1 (0.8%)	4 (2.4%)		0 (0.0%)	0 (0.0%)		1 (2.9%)	1 (3.6%)	
Alcohol	10 (8.3%)	6 (3.5%)		3 (6.7%)	2 (2.5%)		2 (5.9%)	0 (0.0%)	
Other	12 (10.0%)	8 (4.7%)		5 (11.1%)	3 (3.8%)		6 (17.6%)	0 (0.0%)	
HBV-DNA replication≥10^3			0.654			0.136			0.449
No	76 (63.3%)	112 (65.9%)		34 (75.6%)	50 (62.5%)		26 (76.5%)	19 (67.9%)	
Yes	44 (36.7%)	58 (34.1%)		11 (24.4%)	30 (37.5%)		8 (23.5%)	9 (32.1%)	
TBIL (μmol/L)	14 (12, 18)	15 (12, 21)	0.311	15 (13, 18)	15 (12, 19)	0.928	15 (11, 20)	14 (12, 17)	0.713
Albumin (g/L)	42.4 ± 3.9	41.3 ± 3.9	0.316	40.5 ± 5.1	41.5 ± 4.7	0.307	41.8 ± 3.9	40.1 ± 3.1	0.057
ALT	30 (21, 50)	28 (20, 40)	0.309	31 (23, 38)	34 (22, 51)	0.611	30 (23, 45)	30 (22, 53)	0.983
AST	34 (25, 43)	30 (24, 39)	0.138	36 (28, 52)	36 (26, 45)	0.984	33 (27, 53)	30 (23, 47)	0.369
ALP (U/L)	91 (78, 110)	92 (75, 116)	0.859	100 (74, 131)	98 (75, 117)	0.837	95 (75, 125)	81 (67, 104)	0.065
APTT (s)	27.47 ± 2.21	27.63 ± 2.47	0.546	27.29 ± 3.38	27.35 ± 1.87	0.909	27.72 ± 1.80	28.74 ± 2.77	0.100
PT (s)	11.48 ± 0.75	11.61 ± 0.81	0.172	12.02 ± 1.11	11.54 ± 1.05	0.021	11.81 ± 0.86	11.66 ± 0.67	0.443
FIB (s)	2.38 (2.03, 3.08)	2.54 (2.12, 3.33)	0.190	2.49 (2.19, 3.05)	2.28 (2.01, 2.83)	0.200	2.59 (2.08, 3.20)	2.58 (2.23, 2.93)	0.750
TT (s)	18.81 ± 1.24	18.68 ± 1.49	0.428	18.72 ± 1.39	18.87 ± 1.11	0.537	18.48 ± 1.58	19.34 ± 1.21	0.018
WBC (x109g/L)	5.22 (4.46, 6.21)	5.34 (4.26, 6.07)	0.763	5.00 (4.20, 6.55)	5.30 (4.34, 6.80)	0.456	6.17 (4.59, 6.98)	5.62 (4.77, 6.57)	0.305
PLT (x109g/L)	167 ± 75	158 ± 65	0.299	152 ± 70	153 ± 61	0.968	167 ± 37	165 ± 49	0.851
AFP>400ng/mL			0.250			0.727			0.394
No	92 (76.7%)	120 (70.6%)		35 (77.8%)	60 (75.0%)		23 (67.6%)	16 (57.1%)	
Yes	28 (23.3%)	50 (29.4%)		10 (22.2%)	20 (25.0%)		11 (32.4%)	12 (42.9%)	
BCLC			0.167			0.098			0.896
0	14 (11.7%)	27 (15.9%)		4 (8.9%)	18 (22.5%)		3 (8.8%)	4 (14.3%)	
A	78 (65.0%)	109 (64.1%)		29 (64.4%)	44 (55.0%)		23 (67.6%)	17 (60.7%)	
B	15 (12.5%)	10 (5.9%)		6 (13.3%)	4 (5.0%)		5 (14.7%)	5 (17.9%)	
C	13 (10.8%)	24 (14.1%)		6 (13.3%)	14 (17.5%)		3 (8.8%)	2 (7.1%)	

Abbreviations: iTLSs, intratumoral tertiary lymphoid structures; HBV, hepatitis B virus; HCV, hepatitis C virus; HBV-DNA, hepatitis B virus-deoxyribonucleic acid; TBIL, total bilirubin; ALP, alkaline phosphatase; AST, aspartate aminotransferase; ALT, alanine aminotransferase; APTT, activated partial thromboplastin time; PT, prothrombin time; FIB, fibrinogen; TT, thrombin time; WBC, white blood cells; PLT, platelet; AFP, alpha-fetoprotein; BCLC, Barcelona Clinic Liver Cancer.

Table 3 Univariate and Multivariate Analysis of Imaging Features in the Training Cohort by iTLSs Status

Features	Univariate			Multivariate		
	iTLSs-n = 120	iTLSs+n = 170	p	OR	95% CI	p
Size (cm)	4.63 ± 2.37	3.99 ± 2.04	0.018			0.741
Regular shape			0.766			
No	97 (80.8%)	135 (79.4%)				
Yes	23 (19.2%)	35 (20.6%)				
Intratumor fat			0.344			
No	95 (79.2%)	142 (83.5%)				
Yes	25 (20.8%)	28 (16.5%)				
Arterial phase peritumoral enhancement			0.088			
No	96 (80.0%)	121 (71.2%)				
Yes	24 (20.0%)	49 (28.8%)				
Complete capsule			0.881			
No	88 (73.3%)	126 (74.1%)				
Yes	32 (26.7%)	44 (25.9%)				
Intratumor necrosis or ischemia (>20%)			0.298			
No	90 (75.0%)	118 (69.4%)				
Yes	30 (25.0%)	52 (30.6%)				
Intratumor necrosis or ischemia (>50%)			0.688			
No	103 (85.8%)	143 (84.1%)				
Yes	17 (14.2%)	27 (15.9%)				
Satellite nodule			0.221			
No	104 (86.7%)	155 (91.2%)				
Yes	16 (13.3%)	15 (8.8%)				
Peritumoral HBP hypointensity			0.476			
No	72 (60.0%)	109 (64.1%)				
Yes	48 (40.0%)	61 (35.9%)				
Tumor in vein			0.170			
No	110 (91.7%)	147 (86.5%)				
Yes	10 (8.3%)	23 (13.5%)				
Rim APHE			0.639			
No	94 (78.3%)	137 (80.6%)				
Yes	26 (21.7%)	33 (19.4%)				
Mosaic structure			0.445			
No	42 (35.0%)	67 (39.4%)				
Yes	78 (65.0%)	103 (60.6%)				
Intratumor artery			0.016			0.570
No	57 (47.5%)	105 (61.8%)				
Yes	63 (52.5%)	65 (38.2%)				
Intratumor hemorrhage			<0.001	0.231	0.140 ~ 0.380	<0.001
No	42 (35.0%)	119 (70.0%)				
Yes	78 (65.0%)	51 (30.0%)				

Abbreviations: iTLSs, intratumoral tertiary lymphoid structures; HBP, hepatobiliary phase; APHE, arterial phase hyperenhancement.

TTR than the iTLSs- group (p = 0.036, 0.043). Furthermore, among iTLSs+ patients, those receiving TKI-ICI therapy had significantly longer TTR compared to those without therapy (p = 0.035, 0.036), while no significant difference was observed in the iTLSs- group (p = 0.711, 0.632; Figure 6).

Discussion

In this study, we developed and validated an interpretable ML model using radiomics features extracted from SWI sequence to predict iTLSs status in HCC. Previous literatures reported the use of SWI to assess microvascular invasion

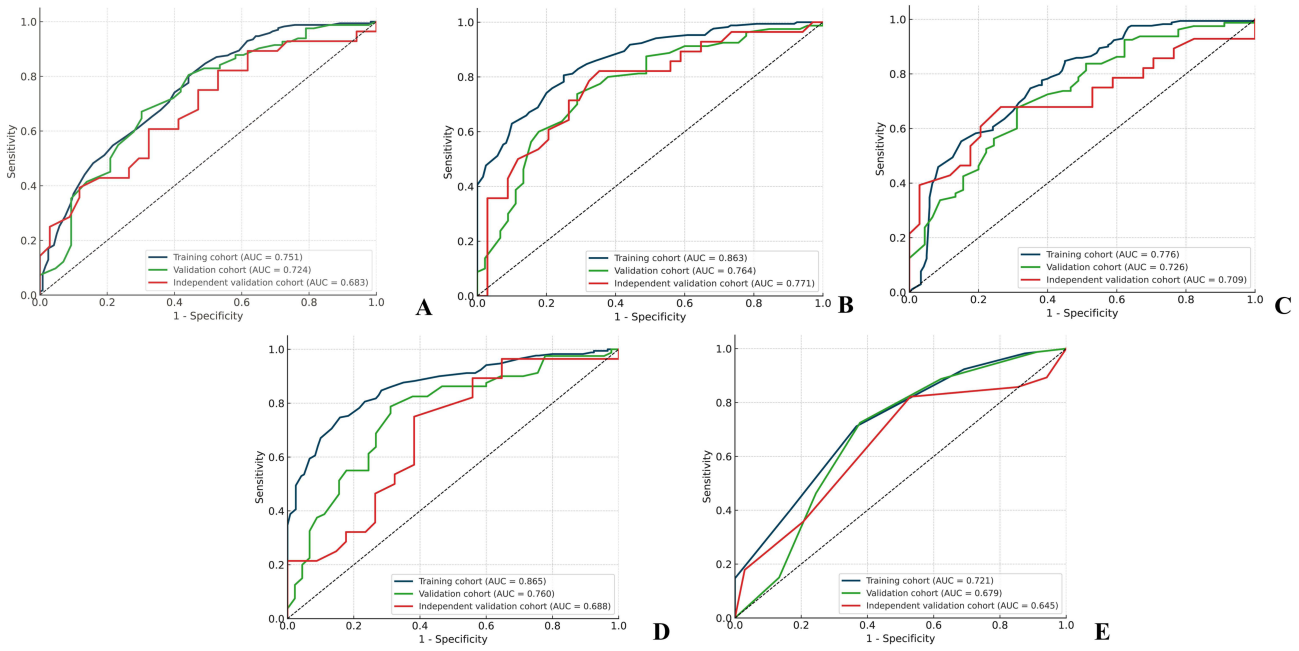

Figure 3 ROC curves of five ML algorithms—LR (**A**), RF (**B**), SVM (**C**), XGBoost (**D**), and KNN (**E**)—for predicting iTLSs in HCC. Each plot includes ROC curves for the training set (blue lines), validation set (green lines), and independent validation set (red lines). The RF algorithm showed superior predictive ability in independent validation cohort, resulting in an AUC value of 0.771 (95% CI: 0.641–0.884).

Abbreviations: ROC, receiver operating characteristic; ML, machine learning; LR, logistic regression; RF, random forest; SVM, support vector machine; XGBoost, extreme gradient boosting; KNN, K-nearest neighbors; iTLSs, intratumoral tertiary lymphoid structures; HCC, hepatocellular carcinoma.

and histopathologic indexes in HCC,[22,23] but the correlation between SWI and iTLSs has not been reported. Our result indicated that the radiomics model could effectively predict iTLSs+ preoperatively across all cohorts. This underscores the potential of radiomics model as a reliable, non-invasive tool to identify iTLSs+, which are associated with a favorable

Table 4 Predictive Performance Metrics of Five Machine Learning Algorithms

Machine Learning Algorithm	Group	AUC	95% CI	Sensitivity	Specificity	Accuracy	PPV	NPV	F1-Score
LR	Training cohort	0.751	0.694~0.805	0.847	0.508	0.707	0.709	0.701	0.772
	Validation cohort	0.724	0.626~0.817	0.829	0.465	0.704	0.747	0.588	0.786
	Independent validation cohort	0.683	0.540~0.809	0.821	0.471	0.629	0.561	0.762	0.667
RF	Training cohort	0.863	0.823~0.901	0.800	0.750	0.779	0.819	0.726	0.810
	Validation cohort	0.764	0.674~0.848	0.775	0.644	0.728	0.795	0.617	0.785
	Independent validation cohort	0.771	0.641~0.883	0.786	0.676	0.726	0.667	0.793	0.721
SVM	Training cohort	0.776	0.719~0.830	0.800	0.567	0.703	0.723	0.667	0.760
	Validation cohort	0.726	0.628~0.816	0.738	0.533	0.664	0.738	0.533	0.738
	Independent validation cohort	0.709	0.552~0.839	0.679	0.559	0.613	0.559	0.679	0.613
XGBoost	Training cohort	0.865	0.822~0.905	0.806	0.767	0.790	0.830	0.736	0.818
	Validation cohort	0.760	0.672~0.846	0.788	0.689	0.752	0.818	0.646	0.803
	Independent validation cohort	0.688	0.547~0.813	0.500	0.676	0.597	0.560	0.622	0.528
KNN	Training cohort	0.721	0.667~0.780	0.712	0.633	0.679	0.733	0.608	0.722
	Validation cohort	0.679	0.580~0.778	0.725	0.622	0.688	0.773	0.560	0.748
	Independent validation cohort	0.645	0.502~0.768	0.821	0.471	0.629	0.561	0.762	0.667

Abbreviations: AUC, area under the curve; CI, confidence interval; PPV, positive predictive value; NPV, negative predictive value; LR, logistic regression; RF, random forest; SVM, support vector machine; XGBoost, extreme gradient boosting; KNN, K-nearest neighbors.

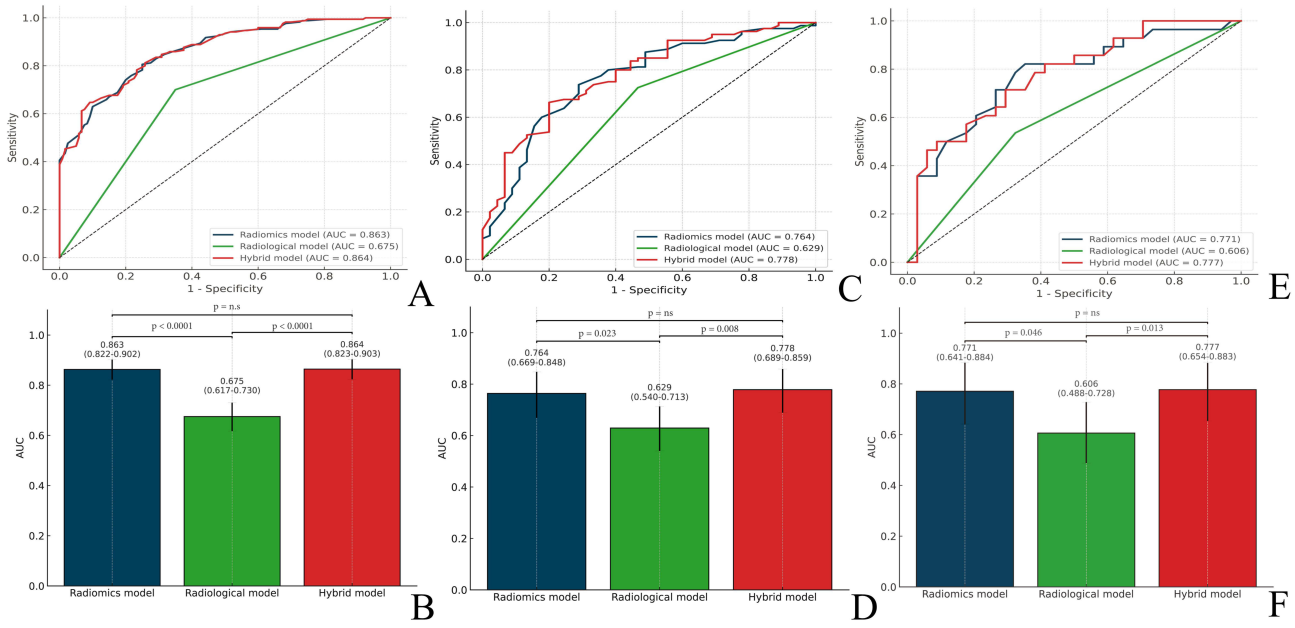

Figure 4 ROC curves based on the RF algorithm to compare different models for predicting iTLSs+ in HCC. Panels (**A** and **B**) represent the performance in the training cohort, (**C** and **D**) in the validation cohort, and (**E and F**) in the independent validation cohort. In all three cohorts, the radiomics models consistently demonstrated predictive performance comparable to that of the hybrid models (all $p > 0.05$), and both outperformed the radiological models (all $p < 0.05$). Blue lines represented radiomics model, green lines represented radiological model, and red lines represented hybrid model.
Abbreviations: ROC, receiver operating characteristic; RF, random forest; iTLSs, intratumoral tertiary lymphoid structures; HCC, hepatocellular carcinoma.

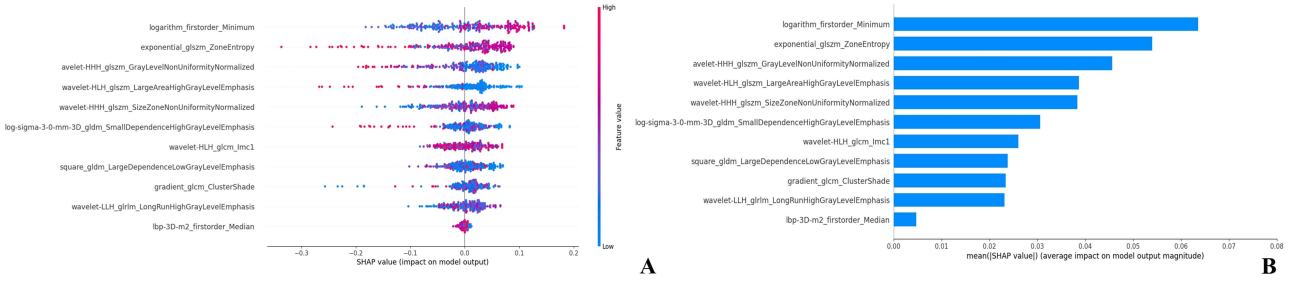

Figure 5 Interpretability of the radiomics model. The SHAP summary plot (**A**) further illustrated the direction and distribution of each feature's influence at the individual patient level. High feature values (in red) of key radiomic variables were generally associated with positive SHAP values, indicating a strong tendency toward predicting iTLSs +. Conversely, low feature values (in blue) tended to contribute negatively to the model output. The SHAP importance diagram (**B**) highlighted the relative contribution of individual variables in differentiating between iTLSs+ and iTLSs-. Features were ranked based on their average absolute SHAP values, with higher values reflecting a greater impact on the model's predictive output.
Abbreviations: SHAP, shapley additive explanations; iTLSs, intratumoral tertiary lymphoid structures.

immune microenvironment and improved patient outcomes. These findings have critical implications for clinical decision-making, enabling early stratification of HCC patients for personalized therapies and facilitating non-invasive prognostic assessment.[8]

This study demonstrated that the absence of intratumoral hemorrhage has certain value in predicting iTLSs+ in HCC, with AUC of 0.606 in the independent validation cohort. These findings are consistent with those of Li et al,[9,10] the underlying mechanism may be related to vascular dysfunction caused by the degradation of collagen and elastin.[24,25] However, the relatively lower predictive performance underscores their limitations. SWI sequences, in particular, pose challenges in terms of observer agreement due to breathing artifacts resulting from long acquisition times,[22] as reflected by a substantial Fleiss kappa value of 0.753. Additionally, visual assessments of intratumoral hemorrhage are inherently subjective, which can restrict their accuracy and reproducibility. As previously reported,[26] inter-observer variability can significantly impact diagnostic outcomes. These limitations highlight the need for more advanced, quantitative methodologies, such as radiomics, which offer greater objectivity and predictive accuracy.

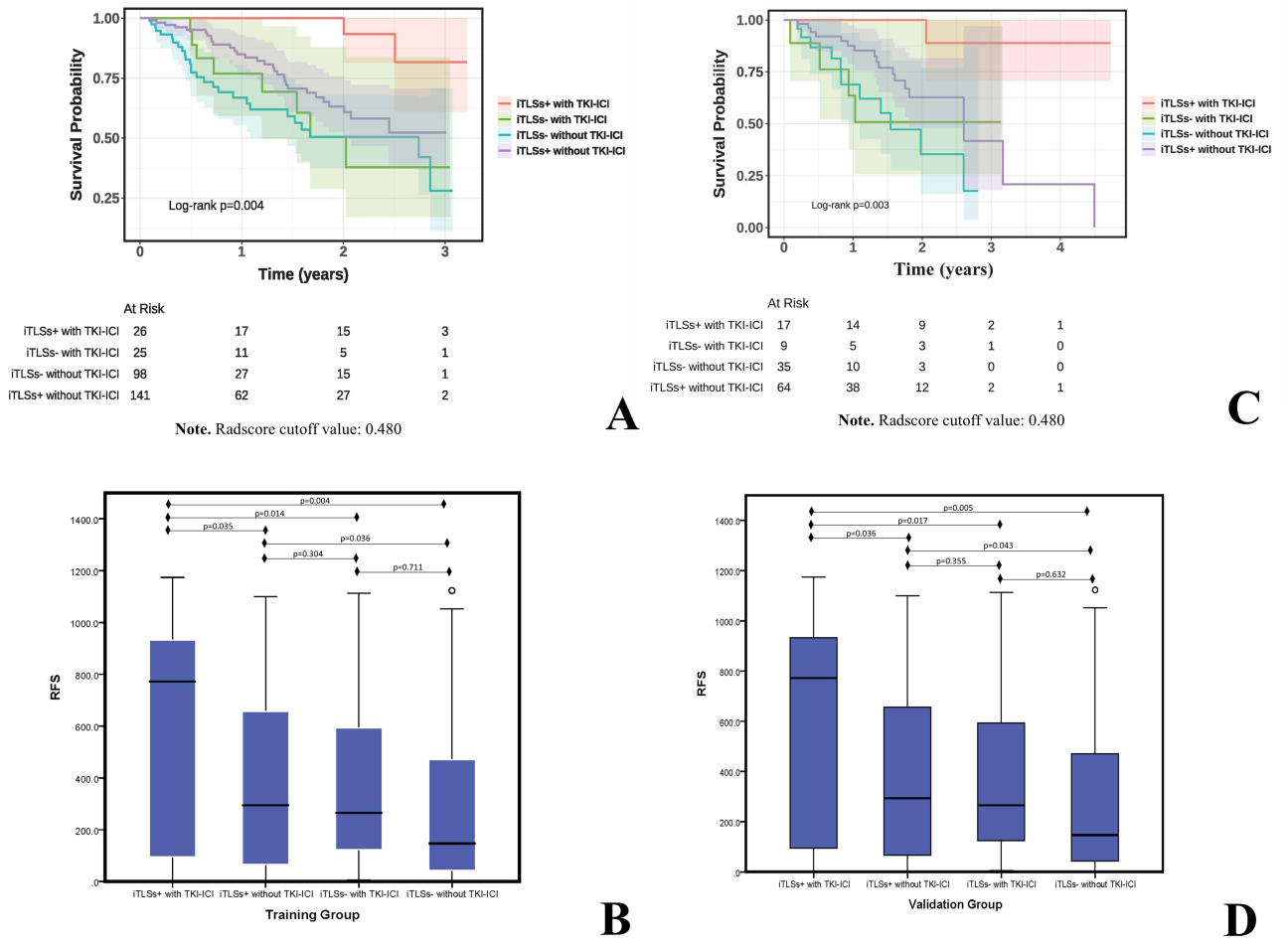

Figure 6 The prediction of prognosis based on radiomics model. (**A and B)** in the training cohort, the patients with iTLSs+ predictor group could benefit from TKI-ICI therapy (all $p < 0.05$), with no significant effect in the iTLSs- predictor group ($p > 0.05$). The prognosis of the iTLSs+ predictor group without TKI-ICI was better than that of the iTLSs- predictor group ($p = 0.036$). (**C and D)** in the validation cohort, the patients with iTLSs+ predictor group could benefit from TKI-ICI therapy (all $p < 0.05$), with no significant effect in the iTLSs- predictor group ($p > 0.05$). The prognosis of the iTLSs+ predictor group without TKI-ICI was better than that of the iTLSs- predictor group ($p = 0.043$).

Abbreviations: iTLSs, intratumoral tertiary lymphoid structures; TKI-ICI, tyrosine kinase inhibitors combined with immune checkpoint inhibitors.

This study explored an SWI-based radiomics model for predicting iTLSs+ in HCC. While its predictive performance was not significantly improved when combined with the radiological model, the radiomics model outperformed the radiological model across all cohorts (all $p < 0.05$). These findings demonstrate the radiomics model's ability to capture subtle tumor heterogeneity and microenvironmental complexities beyond the resolution of the human eye, highlighting its significant potential in assessing the tumor immune microenvironment. Consistent with existing studies, radiomics techniques have been widely applied to assess biological characteristics such as proliferation, angiogenesis, and immune cell infiltration of HCC.[27–30] However, our study added a novel perspective by using SWI to investigate the immune microenvironment in HCC. SWI is uniquely sensitive to abnormalities in tumor microvascular structure,[31] allowing for the detection of subtle features like hypoxia status,[32] which are critical for reflecting immune escape in tumors, hypoxia triggers a cascade of events that promote tumor growth, enhance resistance to the anti-tumor immune response and instigate tumor angiogenesis.[33]

The "black-box" nature and limited interpretability of radiomics model hinder their widespread clinical use, as clinicians often hesitate to trust their predictions.[34] Using the SHAP method, we validated that logarithm_firstorder_Minimum and exponential_GLSZM_ZoneEntropy are important features for predicting iTLSs+. First, the logarithm_firstorder_Minimum feature represents the minimum signal intensity,[16] A higher value indicates the absence of pronounced low-signal regions within the tumor, suggesting more uniform blood perfusion, which may facilitate the formation of iTLSs.[35] Second, the

feature exponential_GLSZM_ZoneEntropy reflects the complexity of gray-level zone size distribution within the tumor,[36] high ZoneEntropy values may capture a diverse range of signal intensities resulting from microvascular remodeling, hemorrhage, and fibrosis, which may facilitate iTLSs development.[37]

In HCC, the iTLSs+ has been associated with improved prognosis and enhanced efficacy of immunotherapy.[38–41] Although TKI-ICI therapy benefits some patients, reliable clinical biomarkers to identify responders remain lacking. Based on our SWI radiomics model, the iTLSs+ predictor group showed significantly improved TTR in both training and validation cohorts, especially among those receiving TKI-ICI therapy. This aligns with recent findings by Li et al,[10] who reported that high-risk iTLSs+ patients identified by combined radiomics and clinical-radiological models could benefit from TKI-ICI after surgery. Notably, our study proposed a single-sequence SWI-based model with strong predictive performance and clear survival differences across cohorts. This simpler approach may facilitate treatment decisions in resource-limited settings, reducing both cost and potential side effects.

To further enhance methodological transparency and reproducibility, we referred to established frameworks such as the Radiomics Quality Score (RQS)[42] and the METhodological RadiomICs Score (METRICS).[43] Our study addressed several key RQS items, including standardized imaging protocols, reproducible segmentation, robust feature selection, validation in an independent cohort, biological plausibility through the association with iTLSs and treatment response, and comparisons with traditional models. However, phantom studies and open data/code availability were not feasible in the present work, representing important areas for future improvement.

This study had several limitations. First, as a single-center, retrospective study, its findings might lack generalizability, and the absence of multicenter validation limited robustness. Future work will therefore focus on prospective, multicenter studies. Second, although the model predicted iTLSs presence, it did not assess their maturity or function; incorporating histopathological correlates such as immune cell quantification or spatial transcriptomics could enhance biological relevance. Third, the subgroup analysis of patients receiving TKI-ICI therapy (n=77) was limited by the relatively small sample size, which might reduce statistical power; thus, these findings should be considered exploratory and require validation in larger, multicenter, prospective cohorts. Finally, manual VOI segmentation might introduce variability, and future efforts could leverage semi-automated or AI-assisted tools to improve reproducibility.

In conclusion, this study demonstrated the potential of SWI-based radiomics for non-invasive assessment of iTLSs in HCC. While the findings were promising, further research and external validation are required before clinical application. These results offer a basis for future work toward individualized diagnosis and treatment.

Data Sharing Statement

The datasets generated and/or analyzed during the current study are not publicly available but are available from the corresponding authors, Dr. Wei Chen and Xiaoming Li, upon reasonable request.

Ethics Approval and Informed Consent

The study was approved by the Institutional Review Board of the Southwest Hospital which waived the requirement for informed patient consent (approval no. KY2023107). It was registered in the Research Registry (researchregistry10321). All methods were carried out in accordance with relevant guidelines and regulations.

Author Contributions

All authors made a significant contribution to the work reported, whether that is in the conception, study design, execution, acquisition of data, analysis and interpretation, or in all these areas; took part in drafting, revising or critically reviewing the article; gave final approval of the version to be published; have agreed on the journal to which the article has been submitted; and agree to be accountable for all aspects of the work.

Funding

This work was supported by the Program of the National Natural Science Foundation of Chongqing (CSTB2022NSCQMSX1371) and Chongqing Science and Technology Development Foundation (No. CSTB2024NSCQ-KJFZZDX0036).

Disclosure

The authors declare no competing interests in this work.

References

1. Bray F, Laversanne M, Sung H, et al. Global cancer statistics 2022: GLOBOCAN estimates of incidence and mortality worldwide for 36 cancers in 185 countries. *Ca A Cancer J Clinicians*. 2024;74(3):229–263. doi:10.3322/caac.21834
2. Singal AG, Kanwal F, Llovet JM. Global trends in hepatocellular carcinoma epidemiology: implications for screening, prevention and therapy. *Nat Rev Clin Oncol*. 2023;20(12):864–884. doi:10.1038/s41571-023-00825-3
3. Qin S, Chen M, Cheng AL, et al. Atezolizumab plus bevacizumab versus active surveillance in patients with resected or ablated high-risk hepatocellular carcinoma (IMbrave050): a randomised, open-label, multicentre, Phase 3 trial. *Lancet*. 2023;402(10415):1835–1847. doi:10.1016/s0140-6736(23)01796-8
4. Brown ZJ, Greten TF, Heinrich B. Adjuvant treatment of hepatocellular carcinoma: prospect of immunotherapy. *Hepatology*. 2019;70(4):1437–1442. doi:10.1002/hep.30633
5. Jin MZ, Jin WL. The updated landscape of tumor microenvironment and drug repurposing. *Signal Transduction Targeted Ther*. 2020;5(1):166. doi:10.1038/s41392-020-00280-x
6. Elhanani O, Ben-Uri R, Keren L. Spatial profiling technologies illuminate the tumor microenvironment. *Cancer Cell*. 2023;41(3):404–420. doi:10.1016/j.ccell.2023.01.010
7. Sautès-Fridman C, Petitprez F, Calderaro J, Fridman WH. Tertiary lymphoid structures in the era of cancer immunotherapy. *Nat Rev Cancer*. 2019;19(6):307–325. doi:10.1038/s41568-019-0144-6
8. Shu DH, Ho WJ, Kagohara LT, et al. Immunotherapy response induces divergent tertiary lymphoid structure morphologies in hepatocellular carcinoma. *Nat Immunol*. 2024;25(11):2110–2123. doi:10.1038/s41590-024-01992-w
9. Li P, Liang Y, Zeng B, et al. Preoperative prediction of intra-tumoral tertiary lymphoid structures based on CT in hepatocellular cancer. *Eur J Radiol*. 2022;151:110309. doi:10.1016/j.ejrad.2022.110309
10. Li Y, Li X, Xiao X, et al. A novel hybrid model for predicting tertiary lymphoid structures and targeted immunotherapy outcomes in hepatocellular carcinoma: a multicenter retrospective study. *Eur Radiol*. 2024;35(6):3206–3222. doi:10.1007/s00330-024-11255-9
11. Karimy JK, Reeves BC, Kahle KT. Targeting TLR4-dependent inflammation in post-hemorrhagic brain injury. *Expert Opinion Therapeut Targets*. 2020;24(6):525–533. doi:10.1080/14728222.2020.1752182
12. Agoro R, Taleb M, Quesniaux VFJ, Mura C. Cell iron status influences macrophage polarization. *PLoS One*. 2018;13(5):e0196921. doi:10.1371/journal.pone.0196921
13. Huang C, Xiao X, Guo M, et al. Value of susceptibility-weighted imaging in differentiating benign from malignant portal vein thrombosis. *Quantit Imaging Med Surg*. 2023;13(4):2688–2696. doi:10.21037/qims-22-350
14. Tao R, Zhang J, Dai Y, et al. Characterizing hepatocellular carcinoma using multi-breath-hold two-dimensional susceptibility-weighted imaging: comparison to conventional liver MRI. *Clin. Radiol*. 2012;67(12):e91–7. doi:10.1016/j.crad.2012.08.015
15. Li C, Hu J, Zhou D, et al. Differentiation of bland from neoplastic thrombus of the portal vein in patients with hepatocellular carcinoma: application of susceptibility-weighted MR imaging. *BMC Cancer*. 2014;14(1):590. doi:10.1186/1471-2407-14-590
16. Mayerhoefer ME, Materka A, Langs G, et al. Introduction to radiomics. *J Nuclear Med*. 2020;61(4):488–495. doi:10.2967/jnumed.118.222893
17. Chan AWH, Zhong J, Berhane S, et al. Development of pre and post-operative models to predict early recurrence of hepatocellular carcinoma after surgical resection. *J Hepatol*. 2018;69(6):1284–1293. doi:10.1016/j.jhep.2018.08.027
18. Cerny M, Chernyak V, Olivié D, et al. LI-RADS version 2018 ancillary features at MRI. *Radiographics*. 2018;38(7):1973–2001. doi:10.1148/rg.2018180052
19. Li Y, Chen Y, Wu Z, et al. Noninvasive MRI imaging feature-based prediction of intratumoral tertiary lymphoid structure maturity in hepatocellular carcinoma: a multicenter retrospective study. *Eur Radiol*. 2025. doi:10.1007/s00330-025-11902-9
20. Wei Z, Bai X, Xv Y, et al. A radiomics-based interpretable machine learning model to predict the HER2 status in bladder cancer: a multicenter study. *Insights Into Imaging*. 2024;15(1):262. doi:10.1186/s13244-024-01840-3
21. Landis JR, Koch GG. The measurement of observer agreement for categorical data. *Biometrics*. 1977;33(1):159–174. doi:10.2307/2529310
22. Geng Z, Wang S, Ma L, et al. Prediction of microvascular invasion in hepatocellular carcinoma patients with MRI radiomics based on susceptibility weighted imaging and T2-weighted imaging. *La Radiologia Medica*. 2024;129(8):1130–1142. doi:10.1007/s11547-024-01845-4
23. Geng Z, Zhang Y, Wang S, et al. Radiomics analysis of susceptibility weighted imaging for hepatocellular carcinoma: exploring the correlation between histopathology and radiomics features. *Magnet Reson Med Sci*. 2021;20(3):253–263. doi:10.2463/mrms.mp.2020-0060
24. Feng Z, Li H, Zhao H, et al. Preoperative CT for characterization of aggressive macrotrabecular-massive subtype and vessels that encapsulate tumor clusters pattern in hepatocellular carcinoma. *Radiology*. 2021;300(1):219–229. doi:10.1148/radiol.2021203614
25. Maehara J, Masugi Y, Abe T, et al. Quantification of intratumoral collagen and elastin fibers within hepatocellular carcinoma tissues finds correlations with clinico-patho-radiological features. *Hepatol Res*. 2020;50(5):607–619. doi:10.1111/hepr.13484
26. Obuchowicz R, Oszust M, Piorkowski A. Interobserver variability in quality assessment of magnetic resonance images. *BMC Med Imaging*. 2020;20(1):109. doi:10.1186/s12880-020-00505-z
27. Wang G, Ding F, Chen K, et al. CT-based radiomics nomogram to predict proliferative hepatocellular carcinoma and explore the tumor microenvironment. *J Transl Med*. 2024;22(1):683. doi:10.1186/s12967-024-05393-3
28. Song LN, Wang B, Cai JL, et al. Stratifying ICIs-responsive tumor microenvironment in HCC: from parsing out immune-hypoxic crosstalk to clinically applicable MRI-radiomics models. *Br. J. Cancer*. 2024;130(8):1356–1364. doi:10.1038/s41416-023-02463-z
29. Feng Z, Li H, Liu Q, et al. CT radiomics to predict macrotrabecular-massive subtype and immune status in hepatocellular carcinoma. *Radiology*. 2023;307(1):e221291. doi:10.1148/radiol.221291
30. Chen S, Feng S, Wei J, et al. Pretreatment prediction of immunoscore in hepatocellular cancer: a radiomics-based clinical model based on Gd-EOB-DTPA-enhanced MRI imaging. *Eur Radiol*. 2019;29(8):4177–4187. doi:10.1007/s00330-018-5986-x

31. Grabner G, Kiesel B, Wöhrer A, et al. Local image variance of 7 Tesla SWI is a new technique for preoperative characterization of diffusely infiltrating gliomas: correlation with tumour grade and IDH1 mutational status. *Eur Radiol*. 2017;27(4):1556–1567. doi:10.1007/s00330-016-4451-y
32. Lu X, Meng L, Zhou Y, et al. Quantitative susceptibility-weighted imaging may be an accurate method for determining stroke hypoperfusion and hypoxia of penumbra. *Eur Radiol*. 2021;31(8):6323–6333. doi:10.1007/s00330-020-07485-2
33. Abou Khouzam R, Brodaczewska K, Filipiak A, et al. Tumor hypoxia regulates immune escape/invasion: influence on angiogenesis and potential impact of hypoxic biomarkers on cancer therapies. *Front Immunol*. 2020;11:613114. doi:10.3389/fimmu.2020.613114
34. Liu Z, Luo C, Chen X, et al. Noninvasive prediction of perineural invasion in intrahepatic cholangiocarcinoma by clinicoradiological features and computed tomography radiomics based on interpretable machine learning: a multicenter cohort study. *Inter J Surg*. 2024;110(2):1039–1051. doi:10.1097/js9.0000000000000881
35. Teillaud JL, Houel A, Panouillot M, et al. Tertiary lymphoid structures in anticancer immunity. *Nat Rev Cancer*. 2024;24(9):629–646. doi:10.1038/s41568-024-00728-0
36. Han YE, Cho Y, Kim MJ, et al. Hepatocellular carcinoma pathologic grade prediction using radiomics and machine learning models of gadoxetic acid-enhanced MRI: a two-center study. *Abdom radiol*. 2023;48(1):244–256. doi:10.1007/s00261-022-03679-y
37. Tang Z, Bai Y, Fang Q, et al. Spatial transcriptomics reveals tryptophan metabolism restricting maturation of intratumoral tertiary lymphoid structures. *Cancer Cell*. 2025. doi:10.1016/j.ccell.2025.03.011
38. Nie Y, Fan H, Li J, et al. Tertiary lymphoid structures: associated multiple immune cells and analysis their formation in hepatocellular carcinoma. *FASEB J*. 2022;36(11):e22586. doi:10.1096/fj.202200269RR
39. Jia W, Shi W, Yao Q, et al. Identifying immune infiltration by deep learning to assess the prognosis of patients with hepatocellular carcinoma. *J Cancer Res Clin Oncol*. 2023;149(14):12621–12635. doi:10.1007/s00432-023-05097-z
40. Calderaro J, Petitprez F, Becht E, et al. Intra-tumoral tertiary lymphoid structures are associated with a low risk of early recurrence of hepatocellular carcinoma. *J Hepatol*. 2019;70(1):58–65. doi:10.1016/j.jhep.2018.09.003
41. Li J, Zhang L, Xing H, et al. The absence of intra-tumoral tertiary lymphoid structures is associated with a worse prognosis and mTOR signaling activation in hepatocellular carcinoma with liver transplantation: a multicenter retrospective study. *Adv Sci*. 2024;11(21):e2309348. doi:10.1002/advs.202309348
42. Lambin P, Leijenaar RTH, Deist TM, et al. Radiomics: the bridge between medical imaging and personalized medicine. *Nat Rev Clin Oncol*. 2017;14(12):749–762. doi:10.1038/nrclinonc.2017.141
43. Kocak B, Akinci D'Antonoli T, Mercaldo N, et al. METhodological RadiomICs score (METRICS): a quality scoring tool for radiomics research endorsed by EuSoMII. *Insights Imaging*. 2024;15(1):8. doi:10.1186/s13244-023-01572-w